Applied Catalysis B: Environmental 245 (2019) 662–671

Contents lists available at ScienceDirect

Applied Catalysis B: Environmental

journal homepage: www.elsevier.com/locate/apcatb

New and stable g-C_3N_4/HAp composites as highly efficient photocatalysts for tetracycline fast degradation

Tianhong Xu[a,1], Rongjiang Zou[b,1], Xiaofang Lei[a], Xuemei Qi[a], Qiang Wu[a,c,*], Weifeng Yao[a,c,*], Qunjie Xu[a,c,*]

[a] Shanghai Key Laboratory of Materials Protection and Advanced Materials in Electric Power, Shanghai Engineering Research Center of Energy-Saving in Heat Exchange Systems, Shanghai University of Electric Power, Shanghai, 200090, PR China
[b] Department of Cardiovascular Surgery, Renji Hospital, School of Medicine, Shanghai Jiao Tong University, Shanghai, 200030, PR China
[c] Shanghai Institute of Pollution Control and Ecological Security, Shanghai, 200092, PR China

ARTICLE INFO

Keywords:
Graphitic carbon nitride (g-C_3N_4)
Hydroxyapatite (HAp)
Tetracycline (TC)
Photocatalysis

ABSTRACT

Photocatalysis is a well-established and green technique for degradation of antibiotics in wastewater. Hydroxyapatite (HAp) has excellent biocompatibility, biological activity, non-toxicity and low cost, and has many applications in biomaterials. Recently, HAp has been reported as an inexpensive green photocatalyst for cleaning some drug contaminations. However, its photocatalytic performance and chemical stability are far from practical applications. In this research, a series of porous hollow hydroxyapatite (HAp) microspheres decorated with small amounts of ultrathin graphitic carbon nitride (g-C_3N_4) were firstly and successfully fabricated by a facile hydrothermal procedure. The experimental results show that as-prepared g-C_3N_4/HAp photocatalysts exhibited evidently enhancement on the photocatalytic activities for the degradation of tetracycline (TC), compared with the corresponding ultrathin g-C_3N_4 and porous hollow HAp microspheres. Notably, g-C_3N_4 (1.5 wt.%)/HAp composite displayed a net high photocatalytic activity for TC degradation (almost 100% within 15 min). Moreover, the as-prepared g-C_3N_4 (1.5 wt.%)/HAp exhibited a good stability in the cyclic runs for the photocatalytic degradation of TC, demonstrating its promising potential as an efficient photocatalyst. An optimum decorating amount of ultrathin g-C_3N_4 onto porous hollow HAp microspheres favors an effective separation of photogenerated electron-hole pairs, which can be responsible for the enhanced photocatalytic performance. In addition, the photocatalytic degradation mechanism for TC was proposed. This fundamental research will provide a promising strategy for the development of highly efficient and compatible photocatalysts with many applications.

1. Introduction

With the rapid development of industry and medicine, the presence of antibiotics in water has raised considerable concerns in the modern society [1,2]. As a typical antibiotic, tetracycline (TC) is usually directly released into the water environment, which brings a negative impact on human health and ecosystem equilibrium [3–5]. Various technologies have been employed to remove and degrade TC, such as physical adsorption [6], biodegradation [7], electrochemical oxidation [8] and photocatalytic degradation [9,10]. Note that traditional removal techniques always bring about difficulty in complete degradation TC [11–13]. Among various other technologies investigated so far, photocatalytic degradation is a well-established and green technique with cost-effective, high-performance and environmentally sustainable alternative for degradation of TC in wastewater [14–16].

As an important type of inorganic functional material, hydroxyapatite ($Ca_{10}(PO_4)_6(OH)_2$, HAp) has captured much attention due to its excellent biocompatibility, bioactivity, non-toxicity, low cost and diverse applications in biomaterials, adsorbents, and ion exchangers [16–21]. More recently, HAp has been confirmed as a cheap and green photocatalyst for degradation of some organic pollutants [14,16]. Nevertheless, the chemical stability and photocatalytic performance is still unsatisfactory in those cases. Thus, further fabricating HAp-based composite photocatalyst with high efficiency and stability will be of

* Corresponding authors at: Shanghai Key Laboratory of Materials Protection and Advanced Materials in Electric Power, Shanghai Engineering Research Center of Energy-Saving in Heat Exchange Systems, Shanghai University of Electric Power, Shanghai, 200090, PR China.
E-mail addresses: qiangwu@shiep.edu.cn (Q. Wu), weifeng@shiep.edu.cn (W. Yao), xuqunjie@shiep.edu.cn (Q. Xu).
[1] These authors contributed equally to this paper.

https://doi.org/10.1016/j.apcatb.2019.01.020
Received 29 November 2018; Received in revised form 1 January 2019; Accepted 8 January 2019
Available online 08 January 2019
0926-3373/

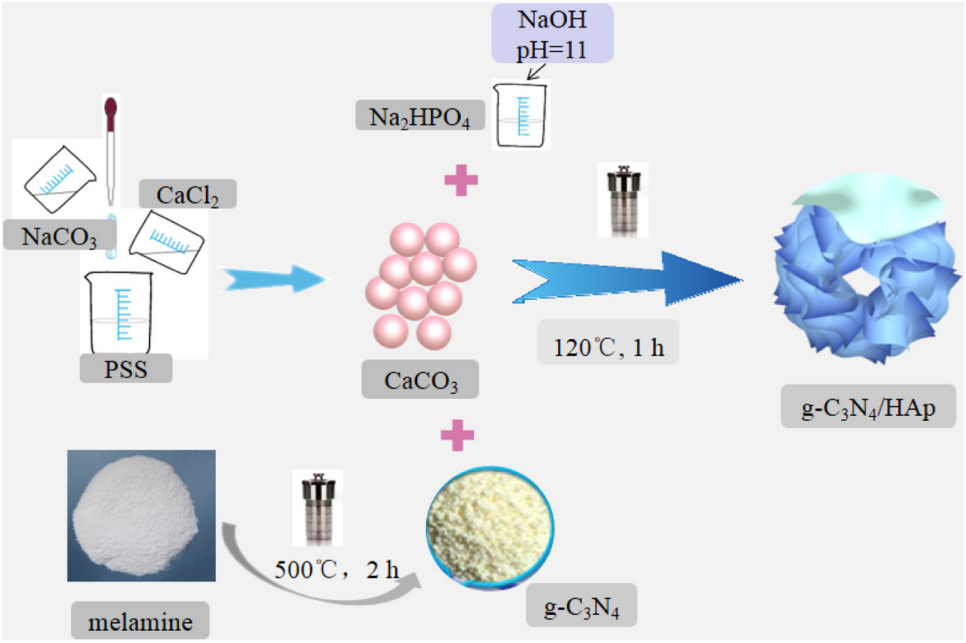

Scheme 1. Schematic illustration for the synthesis of g-C_3N_4/HAp composites.

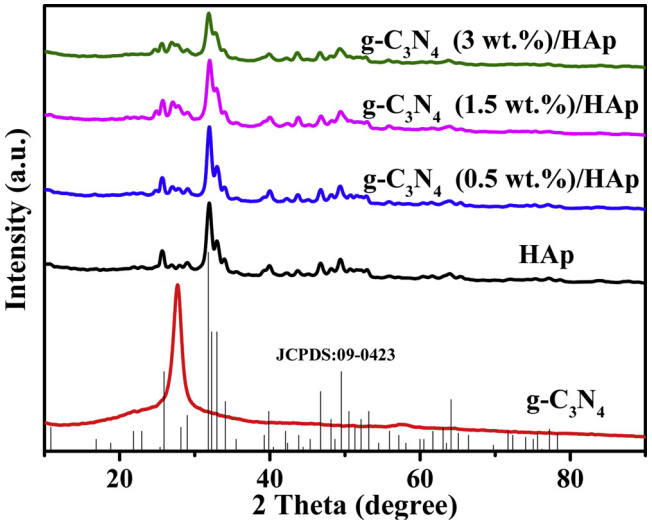

Fig. 1. XRD patterns of g-C_3N_4, HAp, and various g-C_3N_4/HAp composites.

great interest.

Note that in recent years graphitic carbon nitride (g-C_3N_4) has sparked a great deal of interest in photocatalysis and material science [22–25], owning to its versatile properties, such as good photochemical and thermal stability, suitable band gap for visible light absorption, metal-free component, facile synthesis and low cost [26–29]. However, the photocatalytic efficiency of bulk g-C_3N_4 is still not desirable, being a barrier for its practical applications. A feasible way is to fabricate g-C_3N_4 based composite photocatalysts in order to overcome the disadvantages of a single g-C_3N_4 photocatalyst design and enhance the photocatalytic efficiency [30–32].

With regard to the above issues, herein we fabricated a small amount of ultrathin g-C_3N_4 (0.5, 1.5 and 3 wt.%) decorating on the surface of porous hollow HAp microspheres for the first time by a facile hydrothermal method, in attempt to develop a novel and green photocatalyst that with high photocatalytic efficiency and stability. Tetracycline (TC) was used as a model antibiotic for photocatalytic degradation in the present study. In addition, effect of g-C_3N_4 decorating amount, initial TC concentration, and reaction pH value was further investigated. The experimental results confirmed that the as-prepared g-C_3N_4 (1.5 wt.%)/HAp composite can act as promising potential efficient photocatalyst for degradation and removal of TC in wastewater. This fundamental research may cast an alternative approach to designing highly efficient and compatible photocatalyst with many applications.

2. Experimental

2.1. Materials and reagents

Sodium polystyrene sulfonate (PSS) was purchased from MacLean Chemical Reagent. Calcium chloride ($CaCl_2$), sodium carbonate (Na_2CO_3), ethanol (C_2H_5OH), methanol, sodium hydrogen phosphate (Na_2HPO_4), sodium sulfate (Na_2SO_4), sodium hydroxide (NaOH) and melamine were purchased from Sinopharm Chemical Reagent (Shanghai, China). Tetracycline (TC), isopropanol (IPA), ethylene diamine tetraacetic acid (EDTA) and benzoquinone (BQ) were purchased from Aladdin Biochemical Technology Co., Ltd (Shanghai, China). Nafion solution (5 wt.%) was purchased from Alfa Aesar Chemical Co., Ltd (Shanghai, China). All materials were used as received without further purification. Ultrapure water was used as the solvent throughout the experiment.

2.2. Synthesis of ultrathin g-C_3N_4

A given amount of melamine was put into a semi-closed system and subjected to a two-step heat treatment in Muffle furnace. The first heat treatment (heating rate: 2 °C/min) was kept at 773 K in air for 2 h. Followed by was further deamination treatment (heating rate: 2 °C/min) at 793 K in air for another 2 h. Afterwards, the resulting sample was cooled naturally before grinding. Finally, the corresponding grinded sample was calcinated at 793 K in air for 6 h to obtain ultrathin g-C_3N_4.

2.3. Synthesis of g-C_3N_4/HAp composites

Various g-C_3N_4/HAp composites were prepared via a simple hydrothermal route, as shown in Scheme 1. In a typical run, a sacrificial $CaCO_3$ template was firstly prepared using PPS as soft templates [33].

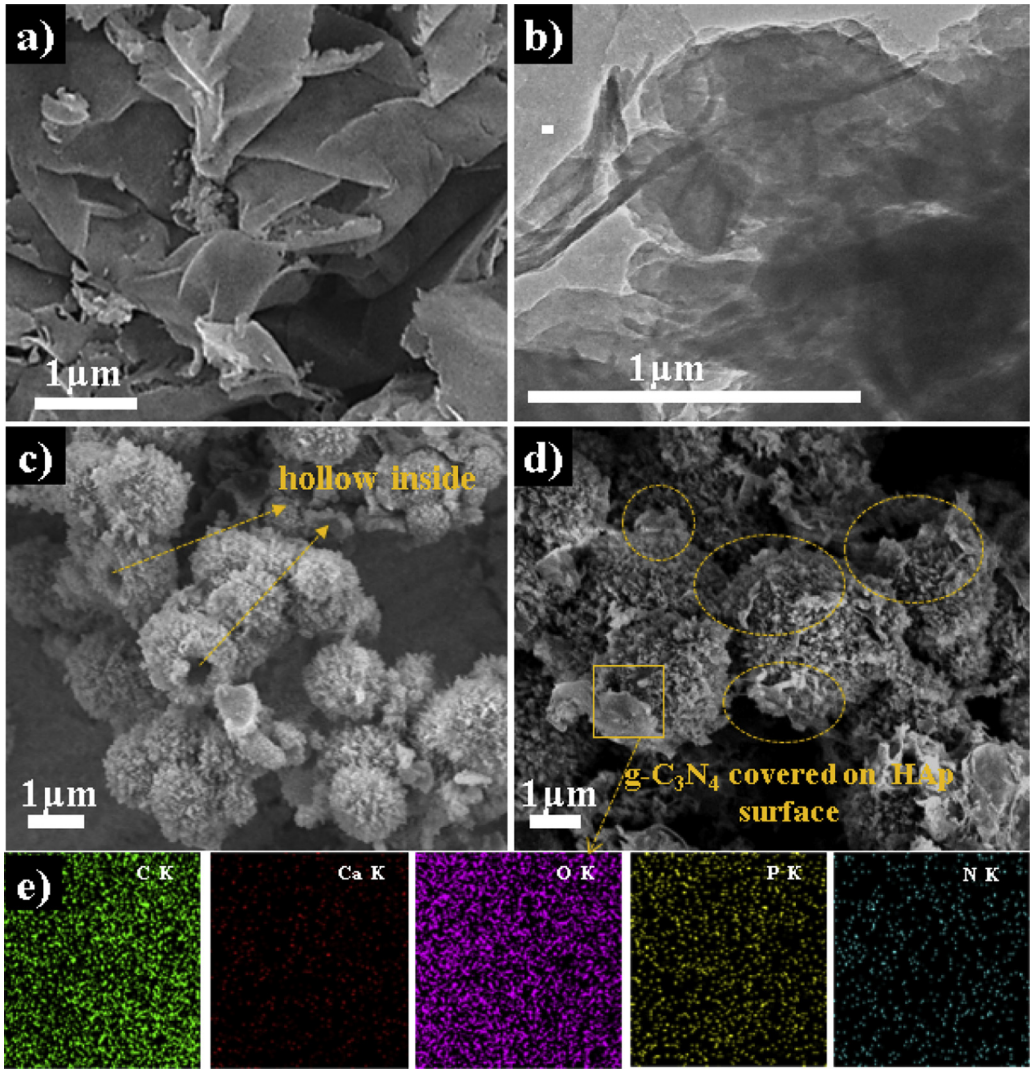

Fig. 2. (a) FE-SEM image and (b) TEM image of g-C_3N_4, (c) FE-SEM image of HAp, (d) FE-SEM image of g-C_3N_4 (1.5 wt.%)/HAp composite, and (e) elemental mapping images of g-C_3N_4 (1.5 wt.%)/HAp.

In brief, $CaCl_2$ solution (30 mL, 0.2 M) was added into PPS solution (300 mL, 10 g/L) under magnetic stirring, followed by was the dropwise addition of Na_2CO_3 (30 mL, 0.2 M) into the prepared mixture. After being magnetically stirred for 1 h, the resulting product was collected by centrifugation and fully washed with deionized water and ethanol. Then target $CaCO_3$ template was obtained after vacuum drying at 333 K overnight. In a next step, 0.2 g of the obtained $CaCO_3$ template was added into Na_2HPO_4 solution (100 mL, 0.2 M) under magnetic stirring. The pH value of the suspension was then adjusted to 11.0 with NaOH solution. Subsequently, the above suspension was transferred into a 200 mL Teflon-lined autoclave, followed by was the addition of 0.5, 1.5 and 3 wt.% g-C_3N_4 into the autoclave, respectively. The autoclave was sealed and hydrothermally treated at 393 K for 1 h. After cooling at room temperature, the corresponding sample was centrifuged and washed by deionized water and ethanol for several times. Finally, the resulting sample was dried under vacuum at 333 K overnight to obtain different g-C_3N_4/HAp composites. Note that porous hollow HAp microspheres (in the absence of ultrathin g-C_3N_4) were also prepared under the similar condition for better comparison.

2.4. Characterization

X-ray diffraction (XRD) analysis was performed using a BRUKER-D8 diffractometer with a Cu-Kα radiation. Fourier transform infrared spectroscopy (FT-IR) was taken with a Spectrum Two™ FT-IR Spectrometer (PerkinElmer, America). Field emission scanning electron microscopy (FE-SEM) measurements were characterized by a Hitachi SU-1500 instrument. Transmission electron microscope (TEM) images were obtained on a JEM-2010 electron microscope operated at 200 kV. X-ray photoelectron spectroscopy (XPS) was determined by an ESCALAB250Xi photoelectron spectrometer with Al kα (1486.6 eV) source and calibrated using the C 1s peak at 284.8 eV. Brunauer-Emmett-Teller (BET) specific surface area was measured using a Gemini VII 2390 instrument. Ultraviolet-visible (UV–vis) diffuse reflectance spectroscopy was conducted on a Shimadzu UV-2550 spectrophotometer. All the electrochemical measurements were performed in a typical three-electrode system using a CHI660E electrochemical station (CH Instruments, Inc., Shanghai). Total organic carbon (TOC) was measured on a TOC analyzer (Shimadzu, Japan). Electron Spin-Resonance spectroscopy (ESR) was carried out to identify the active species using a Bruker EPR A300-10/12 spectrometer. The intermediates of TC were identified by a high performance liquid chromatography–mass spectroscopy (HPLC-MS).

2.5. Photocatalytic experiment for TC and ESR experiments

Photocatalytic TC degradation was performed in a home-made glass reactor at room temperature. In a typical photocatalytic reaction,

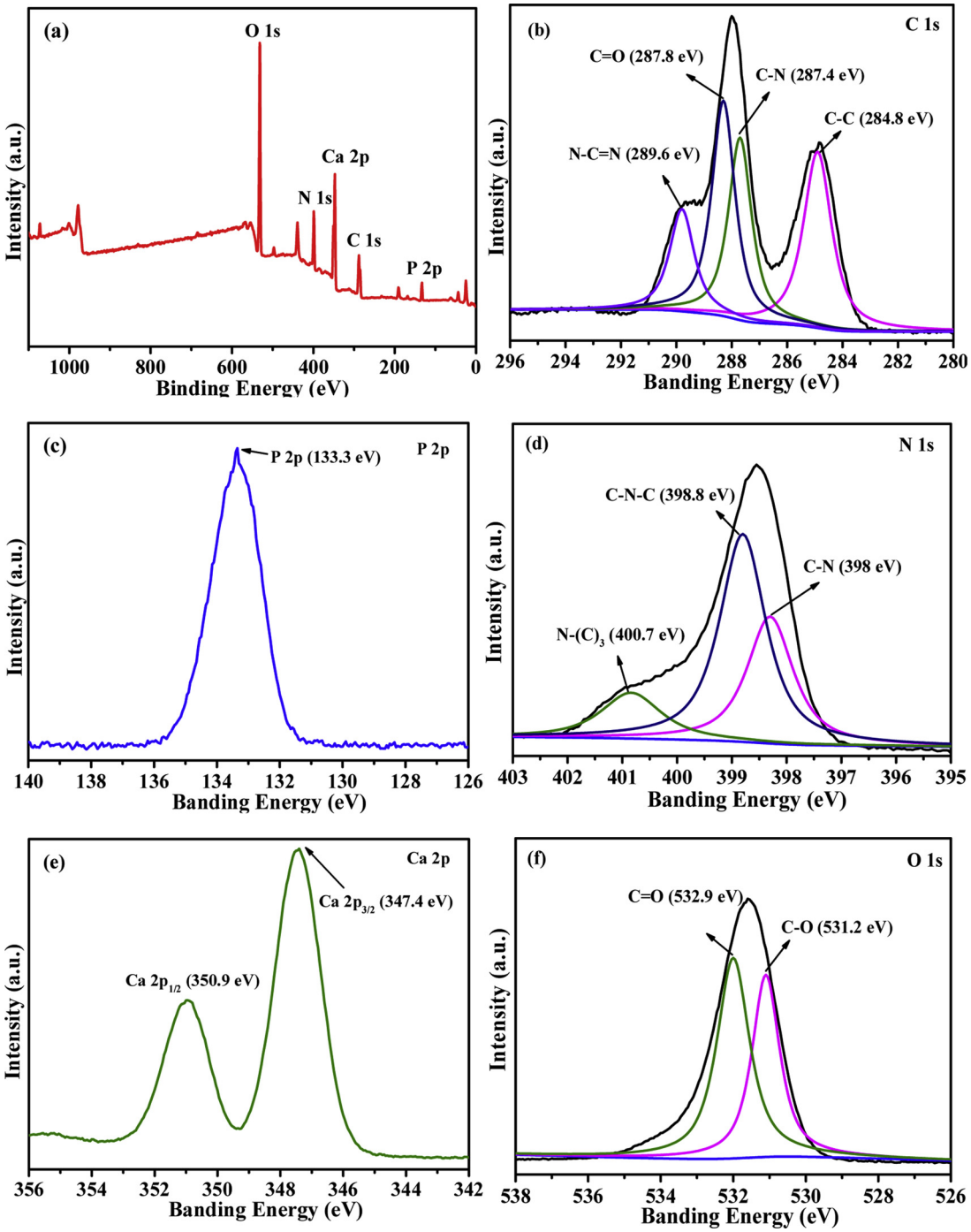

Fig. 3. XPS spectrum of g-C_3N_4 (1.5 wt.%)/HAp composite: (a) survey spectrum, (b) C 1s, (c) P 2p, (d) N 1s, (e) Ca 2p, and (f) O 1s.

100 mg of different g-C_3N_4/HAp photocatalysts were dispersed in a 100 mL TC aqueous solution (20–60 mg/L). Note that a 300 W Xe arc lamp (Perfectlight Co., PLS-SXE 300) with full spectrum irradiation was employed as the light source. Before irradiation, the solution was magnetically stirred in darkness for 30 min to achieve an adsorption-desorption equilibrium between the photocatalyst and TC. In the next step, the lamp was turned on. At given time intervals, 4 mL of suspension was extracted and centrifuged at 8000 rpm for 5 min, and then the supernatant was analyzed to determine its residual concentration by an UV–vis spectrophotometer at the maximal TC adsorption of wavelength of 357 nm. The photocatalytic degradation efficiency (D%) of TC was calculated as follows:

$$D\% = \frac{C0 - C_t}{C0} \times 100\% \quad (1)$$

where C_0 and C_t represent the initial TC concentration and instantaneous TC concentration after a certain irradiation time (t). Effect of several parameters such as reaction pH value, initial TC concentration, and g-C_3N_4 decorating amount was investigated. For comparison, porous hollow HAp microspheres and ultrathin g-C_3N_4 were also adopted for the similar photocatalytic degradation reaction. Furthermore, the recycle experiment was performed to test the durability and recyclability of the obtained photocatalyst. After each cycle, the used photocatalyst was filtrated and washed with deionized water and ethanol in order to remove the residual pollutants, and then dried under vacuum at 333 K overnight for further use.

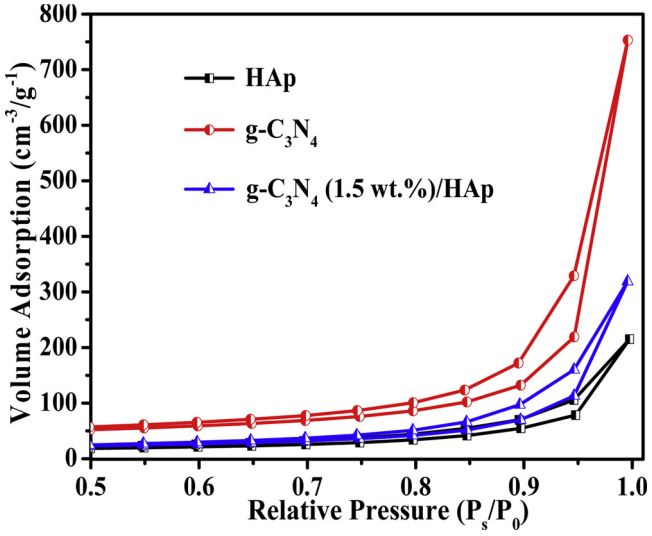

Fig. 4. N_2 adsorption-desorption isotherms of ultrathin g-C_3N_4, porous hollow HAp microspheres, and g-C_3N_4 (1.5 wt.%)/HAp composite.

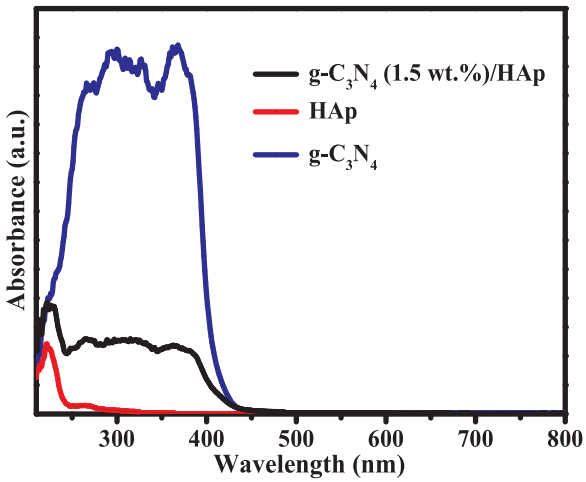

Fig. 5. UV–vis diffusion reflection spectra (DRS) of ultrathin g-C_3N_4, porous hollow HAp microspheres, and g-C_3N_4 (1.5 wt.%)/HAp composite.

In addition, trapping experiments were conducted to elucidate the reasonable photocatalytic mechanism. 2-propanol (IPA), disodium ethylene diamine tetraacetic acid (EDTA), and 1, 4-benzoquinone (BQ) were used as the scavengers to detect the main active species during the photocatalytic process. ESR technique was further applied to identify the active species generated in the photocatalytic process. Note that $^{\cdot}OH$ and $^{\cdot}O_2^-$ radicals can be captured by DMPO, while h^+ radicals can be captured by the TEMPO.

2.6. Photoelectrochemical measurements

The photocurrent measurements, Mott-Schottky (M-S) analyses and electrochemical impedance spectroscopy (EIS) were performed on CHI660E electrochemical workstation (CH Instruments, Inc., Shanghai) by using a standard three-electrode system [34,35] with a Pt foil counter electrode, a standard calomel reference electrode in saturated KCl, and the glassy carbon working electrode. A working electrode homogeneous solution was prepared by dispersing 20 mg photocatalyst in the solution containing 1 mL ethanol and 10 μL nafion, followed by was an ultrasonic treatment for 30 min to obtain a homogeneous slurry. Then dipped 20 μL suspension onto a 1 × 1 cm^2 fluorine-doped tin oxide glass electrode, followed by drying conductive glass in the air for 24 h. The electrolyte was prepared by employing 0.2 M Na_2SO_4 aqueous solution. The photoelectrochemical measurements were measured at 0.5 V bias potential under a 300 W xenon lamp full spectrum (Perfectlight Co., PLS-SXE 300) irradiation.

3. Results and discussion

3.1. Characterization of g-C_3N_4/HAp composites

Fig. 1 shows the XRD patterns of as-prepared g-C_3N_4 (0.5 wt.%)/HAp, g-C_3N_4 (1.5 wt.%)/HAp, and g-C_3N_4 (3 wt.%)/HAp composites. For comparison, Fig. 1 also displays the XRD patterns of the as-prepared pure HAp and g-C_3N_4. Note that the diffraction peaks of g-C_3N_4 are well indexed to a pure g-C_3N_4 phase (JCPDS Card No. 50-1512). As for the as-prepared HAp, all the diffraction peaks match very well the typical hexagonal structured HAp (JCPDS No. 09-0423). As expected, all the XRD patterns of the as-prepared g-C_3N_4/HAp composites match with the polycrystalline structure of HAp and g-C_3N_4, ruling out the formation of any third phase. The results indicate the successful synthesis of g-C_3N_4/HAp composites in the present study. In addition, Fig. S1 demonstrates the FT-IR spectra of the as-prepared g-C_3N_4, HAp, and g-C_3N_4 (1.5 wt.%)/HAp composite. As for HAp, it shows obvious peaks of PO_4^{3-} at 1032, 954, 603, 567 and 465 cm^{-1}, which are the typical characteristic absorption of HAp [36,37]. In case of g-C_3N_4, its spectrum displays several strong peaks from 1800 to 750 cm^{-1}, all of which agree with the distinctive skeletal vibration of the aromatic ring [38]. Compared with the FT-IR spectra of g-C_3N_4 and HAp, the as-prepared g-C_3N_4 (1.5 wt.%)/HAp composite possesses the characteristic peaks of their respective single substance, and this well proofs the successful formation of g-C_3N_4/HAp composites.

The morphologies of the as-prepared samples were further characterized by FE-SEM or TEM technique. Fig. 2a–b shows the corresponding FE-SEM image and TEM image of as-prepared g-C_3N_4, respectively. It is obvious that the typical morphology of g-C_3N_4 showed ultrathin two-dimension layers. As indicated in Fig. 2c, the as-prepared HAp exhibited uniform spherical morphology with an urchin-like structure and its size distribution was ca. 1 μm. It should be noted that the as-prepared HAp sample displayed some broken microspheres, suggesting that HAp microspheres have typical hollow structures. As for g-C_3N_4 (1.5 wt.%)/HAp composite, it is evident from the FE-SEM image that some hollow HAp microspheres were partially wrapped by small amounts of ultrathin g-C_3N_4 (Fig. 2d). Additionally, the corresponding elemental mapping images (Fig. 2e) of g-C_3N_4 (1.5 wt.%)/HAp composite demonstrate the existence of all elements (C, Ca, N, O and P) in the composite together and the uniform distribution of C, Ca, N, O and P on the surface of g-C_3N_4 (1.5 wt.%)/HAp, further confirming the successful synthesis of g-C_3N_4 (1.5 wt.%)/HAp composite in the present study.

The surface chemical composite and electronic states of the as-prepared g-C_3N_4 (1.5 wt.%)/HAp composite were recorded by XPS spectra. As shown in Fig. 3a, the survey spectrum of g-C_3N_4 (1.5 wt.%)/HAp demonstrates the co-existence of C, P, N, Ca and O elements. The C 1s spectrum (Fig. 3b) of g-C_3N_4 (1.5 wt.%)/HAp could be divided into three characteristic peaks, which are attributed to the following functional groups: C—C (284.8 eV), C—N (287.4 eV), C═O (287.8 eV) and N—C═N (289.6 eV) [39,40]. As can be seen in Fig. 3c, the peak at 133.3 eV is ascribed to the electron orbit of P 2p. Note that the N 1s spectrum (Fig. 3d) exhibits three characteristic peaks of nitrogen states including triazine rings C—N—C (398.8 eV), tertiary nitrogen N—$(C)_3$ (400.7 eV) and C—N (398 eV), which are similar to those in the reported literatures [34–36]. Furthermore, the peaks at 347.5 and 350.4 eV (Fig. 3e) correspond to Ca $2p_{3/2}$ and Ca $2p_{1/2}$, respectively. Additionally, the peak of O 1s spectrum located at 531.2 eV and 532.9 eV correspond to C═O and C—O, respectively (Fig. 3f) [41].

The N_2 adsorption-desorption isotherms distributions of the as-prepared porous hollow HAp microspheres, ultrathin g-C_3N_4, and g-

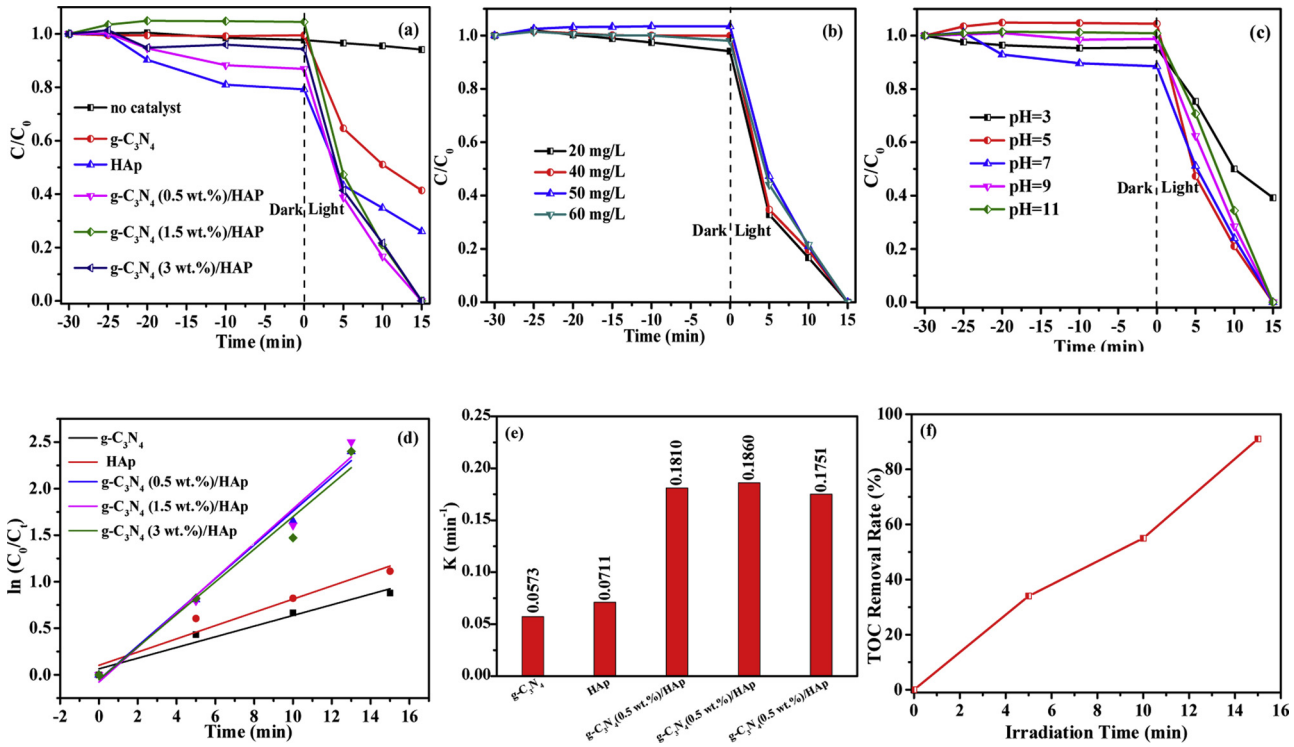

Fig. 6. (a) Effect of decorating amount of ultrathin g-C_3N_4 on TC degradation under 300 W xenon lamp full spectrum irradiation (initial concentration of the TC = 50 mg/L, solution PH = 5, catalyst dosage = 0.1 g), (b) effect of initial TC concentrations on TC degradation over g-C_3N_4 (1.5 wt.%)/HAp under 300 W xenon lamp full spectrum irradiation (solution PH = 5, catalyst dosage = 0.1 g), and (c) effect of reaction pH value on TC degradation over g-C_3N_4 (1.5 wt.%)/HAp under 300 W xenon lamp full spectrum irradiation (initial concentration of the TC = 50 mg/L, catalyst dosage = 0.1 g), (d) the pseudo-first order reaction kinetics, and (e) values of reaction constants over the as-prepared samples, and (f) TOC removal efficiency in the presence of g-C_3N_4 (1.5 wt.%)/HAp under 300 W xenon lamp full spectrum irradiation.

C_3N_4 (1.5 wt.%)/HAp composite are shown in Fig. 4. Clearly, all of the samples possessed a type IV loop at a relative pressure range from 0.4 to 1. It should be pointed out that the BET specific surface area of g-C_3N_4 (1.5 wt.%)/HAp was calculated to be 54.2 m^2/g, much higher than that of porous hollow HAp microspheres (44.2 m^2/g), but lower than that of ultrathin g-C_3N_4 (127.8 m^2/g). It is reasonable to deduct that the enhanced surface area of g-C_3N_4 (1.5 wt.%)/HAp compared with porous hollow HAp microspheres may favor an increase in the number of active sites and thus promotes its photocatalytic activity toward TC degradation.

The UV–vis diffuse reflectance spectra (DRS) of the porous hollow HAp microspheres, ultrathin g-C_3N_4, and g-C_3N_4 (1.5 wt.%)/HAp composite are depicted in Fig. 5. Obviously, porous hollow HAp microspheres exhibit very weak absorption ability in the UV-light region. In contrast, ultrathin g-C_3N_4 reveals broader and stronger absorption ability both in the UV light and visible light region. Importantly, following the modification of a low content of g-C_3N_4 (1.5 wt.%) ultrathin layer anchoring on the surface of porous hollow HAp microspheres, the light harvesting absorption ability was enhanced remarkably both in the UV light and visible light region compared with pure porous hollow HAp microspheres. The above results suggest that g-C_3N_4 (1.5 wt.%)/HAp composite can act as a promising photocatalyst in the wastewater pollutant treatment field.

3.2. Photocatalytic degradation of TC

The photocatalytic performance was investigated by the degradation of TC under various conditions. Several parameters: initial TC concentrations, reaction pH value, and g-C_3N_4 decorating amount were taking into discussion. In addition, the photostability and recycling performance was also evaluated for practical application purpose.

3.2.1. Effect of g-C_3N_4 decorating amount

Fig. 6a illustrates the photocatalytic degradation of TC over various g-C_3N_4/HAp composites under the 300 W xenon lamp irradiation. For comparison, the photocatalytic degradation of TC over the as-prepared porous hollow HAp microspheres and ultrathin g-C_3N_4 were also tested. Note that the blank experiment (direct photolysis without any catalyst) exhibits little photolysis and the corresponding efficiency was only ca. 5.8%. As observed, the as-prepared various photocatalysts demonstrate different photocatalytic degradation rates for TC removal, which was in the order of g-C_3N_4 (1.5 wt.%)/HAp > g-C_3N_4 (0.5 wt.%)/HAp > g-C_3N_4 (3 wt.%)/HAp > porous hollow HAp microspheres > ultrathin g-C_3N_4. Interestingly, the photocatalytic activity could be boosted by decorating of ultrathin g-C_3N_4 on the surface of porous hollow HAp microspheres, and TC was almost completely degraded within 15 min for all g-C_3N_4/HAp composites system. Specifically, the as-prepared g-C_3N_4 (1.5 wt.%)/HAp composite exhibits the highest photocatalytic efficiency, and nearly 100% towards TC was degraded within 15 min. It can be inferred that the decorating amount of ultrathin g-C_3N_4 plays a significantly role in the photodegradation process [42]. Based on the analysis in Fig. 6a, the optimum decorating amount of g-C_3N_4 was found to be 1.5 wt.%. Thus, in the following experiments, g-C_3N_4 (1.5 wt.%)/HAp was used as a model photocatalyst for further investigation.

3.2.2. Effect of initial TC concentrations

As it well known, the initial TC concentration is an important factor to influence final removal efficiency including surface adsorption and photocatalytic performance [43–45]. A series of experiments were performed to investigate the degradation of TC with different initial TC concentrations in the range of 20–60 mg/L over g-C_3N_4 (1.5 wt.%)/HAp photocatalyst. As depicted in Fig. 6b, it can be observed that the initial TC concentration had an unconsidered impact on the adsorption

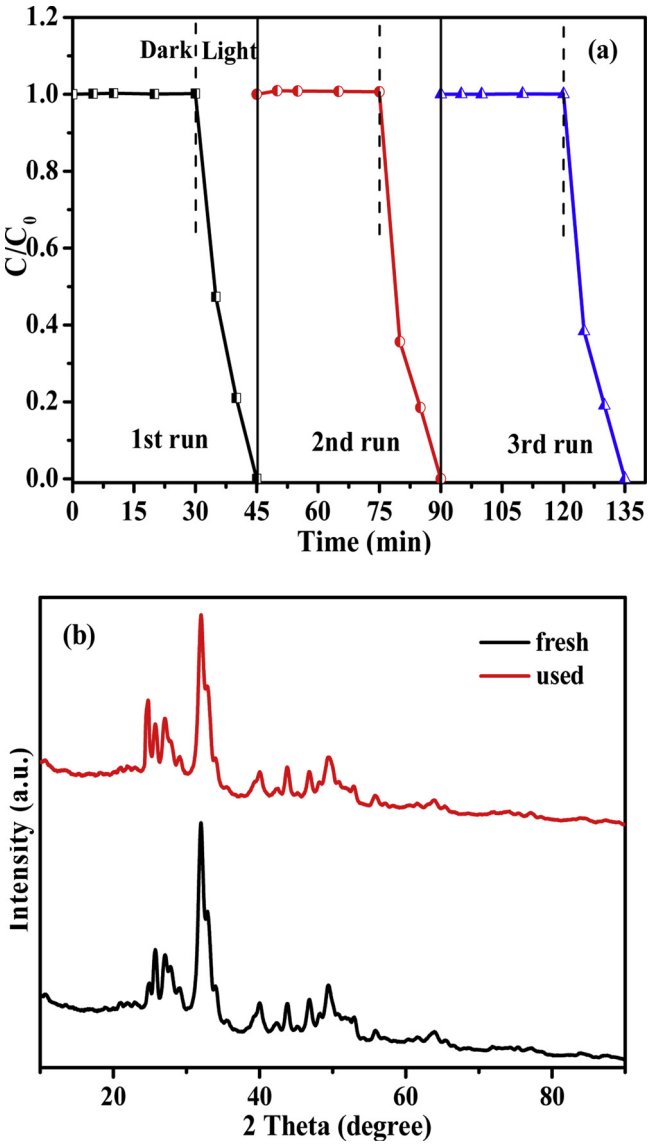

Fig. 7. (a) Cycling runs for the photocatalytic degradation of TC in the presence of g-C_3N_4 (1.5 wt.%)/HAp, and (b) XRD spectra of g-C_3N_4 (1.5 wt.%)/HAp photocatalyst before and after TC degradation.

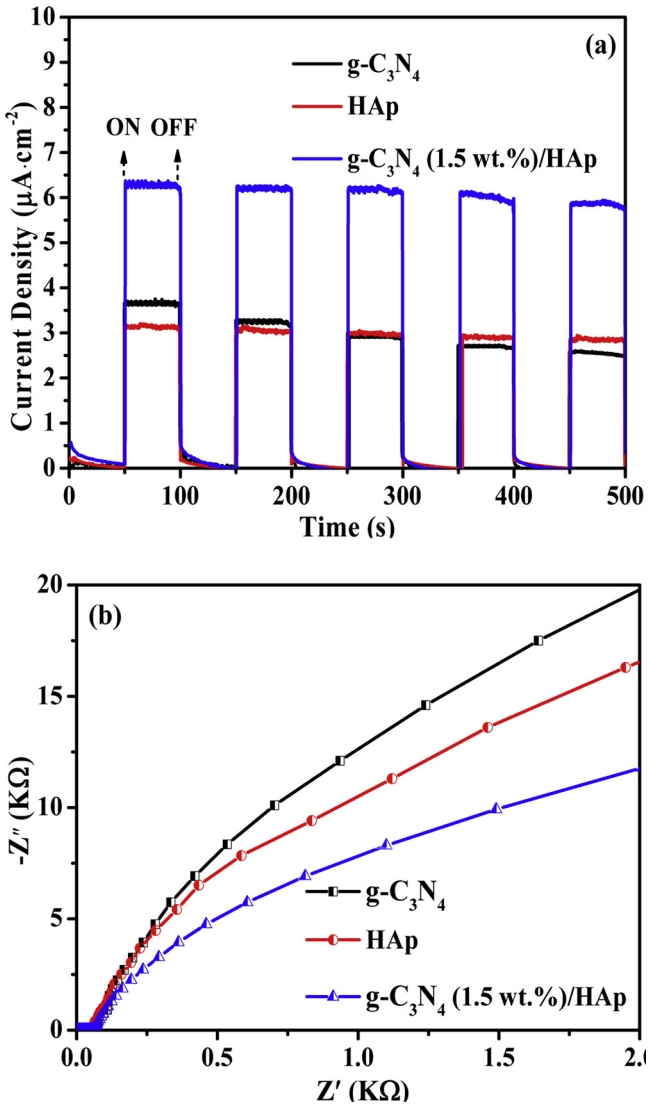

Fig. 8. (a) Transient photocurrent responses of ultrathin g-C_3N_4, porous hollow HAp microspheres, and g-C_3N_4 (1.5 wt.%)/HAp composite, (b) Electrochemical impedance spectroscopy (EIS) analysis of ultrathin g-C_3N_4, porous hollow HAp microspheres, and g-C_3N_4 (1.5 wt.%)/HAp composite.

process in dark period, where 6.0%, 1.0%, 0% and 2.0% of TC were adsorbed at the initial TC concentration accord with 20, 40, 50 and 60 mg/L, respectively. In addition, it is worth noting that TC with different initial concentrations of 20, 40, 50, and 60 mg/L can be completely degraded within 15 min over the as-prepared g-C_3N_4 (1.5 wt.%)/HAp photocatalyst under the xenon lamp irradiation, with the photocatalytic efficiency of ca. 94.0%, 99.0%, 100% and 98.0%, respectively. Therefore, from the results in Fig. 6b, the optimal initial TC concentration was chosen as 50 mg/L in the present study.

In order to further investigate the effect of initial pollutant concentrations on the application of g-C_3N_4 (1.5 wt.%)/HAp in treatment of other antibiotic pollutants, rifampicin (RIF) was also selected as the target pollutant to investigate the photocatalytic degradation performance. From Fig. S2, it is obvious that the initial RIF concentration had no effect on the adsorption process in dark period, however, the initial RIF concentration had a significant impact on the photocatalytic degradation process for RIF. It was confirmed that the photocatalytic efficiency of g-C_3N_4 (1.5 wt.%)/HAp toward antibiotic pollutants are dependent on the type of antibiotic used in the treatment process. Based on all the experimental results, it can be inferred that the obtained g-C_3N_4 (1.5 wt.%)/HAp composite have the universality application for the degradation of various antibiotic pollutants in wastewater.

3.2.3. *Effect of pH value*

As shown in Fig. 6c, a series of pH values were controlled by NaOH (0.1 M) or HCl (0.1 M) to investigate the influence of initial pH (3–11) on TC photocatalytic degradation process. Effect of pH value on TC adsorption onto g-C_3N_4 (1.5 wt.%)/HAp composite is evidenced by dark reaction in Fig. 6c and Fig. S3a. The results show that the adsorption of TC onto g-C_3N_4 (1.5 wt.%)/HAp composite was pH dependent in the range of 3–11 [38]. Specially, a given pH value (pH = 7) had a great effect on the adsorption of TC over g-C_3N_4 (1.5 wt.%)/HAp composite. As shown in Fig. S3b, under acidic conditions (pH < 7), the adsorption of TC onto g-C_3N_4 (1.5 wt.%)/HAp composite increased as the solution pH decreased, which might attribute to the cation exchange process [46,47]. Under alkaline conditions (pH > 7), the adsorption of TC onto g-C_3N_4 (1.5 wt.%)/HAp composite decreased with enhancing alkaline degree, which might ascribe to the repulsive forces between two negatively charged molecules [47]. As observed in Fig. 6c, the photocatalytic degradation efficiency of TC was also slightly influenced by pH value over g-C_3N_4 (1.5 wt.%)/HAp composite under the xenon lamp

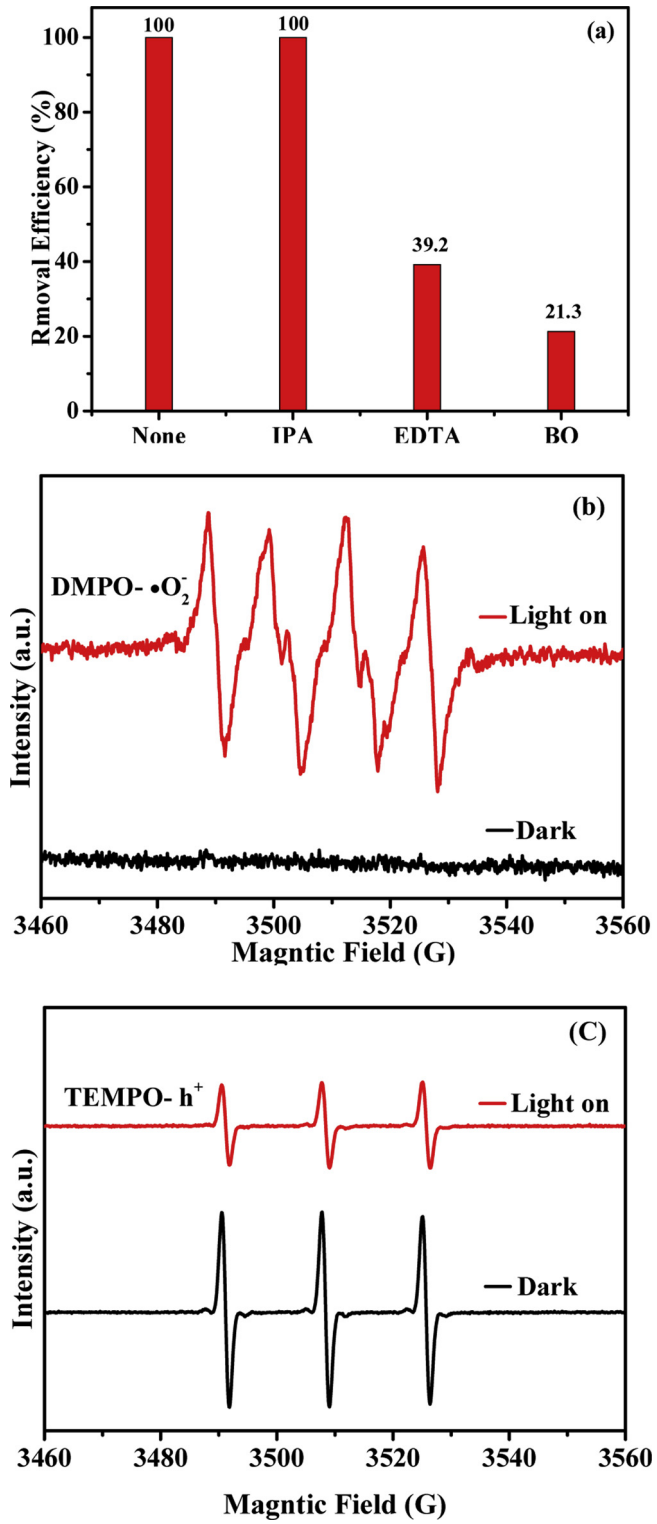

Fig. 9. (a) Photocatalytic activities of g-C_3N_4 (1.5 wt.%)/HAp composite for the degradation of TC in the presence of different scavengers under the xenon lamp irradiation, (b) ESR signals of the DMPO-$\cdot O_2^-$ for g-C_3N_4 (1.5 wt.%)/HAp in the dark and under 300 W xenon lamp full spectrum irradiation, and (c) ESR signals of the TEMPO-h^+ for g-C_3N_4 (1.5 wt.%)/HAp in the dark and under 300 W xenon lamp full spectrum irradiation.

irradiation, and it follows the order of pH (5) > pH (11) > pH (9) > pH (7) > pH (3). Thus, in this research, the optimum pH value was set at 5 owing to the obtained highest photo-activity.

Fig. 6d demonstrates that all the degradation data can fit well with the pseudo-first order correlation ($\ln (C_0/C_t) = \kappa t$), indicating that all the as-prepared photocatalysts follow the first order kinetics. As shown in Fig. 6e, the apparent rate constant of g-C_3N_4 (1.5 wt.%)/HAp is 0.1860 min^{-1}, which is 3.24 and 2.61 times higher than ultrathin g-C_3N_4 and porous hollow HAp microspheres, respectively. The above experimental results provide good proof that an optimum decorating amount of ultrathin g-C_3N_4 onto porous hollow HAp microspheres can act as effective photocatalysts for TC degradation.

Moreover, based on the TOC analysis (Fig. 6f), a mineralization efficiency of 91.0% can be obtained over g-C_3N_4 (1.5 wt.%)/HAp for TC after 15 min irradiation, suggesting g-C_3N_4 (1.5 wt.%)/HAp photocatalyst possessed higher mineralization ability for TC degradation. Note that 91.0% mineralization efficiency was slightly lower than that of degradation efficiency (almost 100%), which suggesting that complete mineralization could not be achieved, and some organic intermediates might generate in the photocatalytic process.

HPLC-MS was further used to analyze intermediates in the photocatalytic reaction process under 300 W xenon lamp full spectrum irradiation (Fig. S4). It is found that there was a characteristic anion peak at m/z 445 belonging to the deprotonated TC. As depicted in Fig. S5, the TC molecular with m/z = 445 could be obtained by active species causing hydrogenation (m/z = 447). With increasing the reaction time, the ions with m/z = 329, m/z = 283, and m/z = 246 were detected, which were due to some loss of functional groups, respectively. Above results suggesting that TC molecule is degraded into CO_2, H_2O and some other intermediates.

3.2.4. Reusability and stability of g-C_3N_4 (1.5 wt.%)/HAp composites

The reusability and stability of g-C_3N_4 (1.5 wt.%)/HAp was investigated by repeating photocatalytic degradation of TC for three times to assess the possibility of the photocatalyst in practical applications. For each cycle, the catalyst was collected by centrifugation, washing and drying before the next run. As shown in Fig. 7, the photocatalytic activity of g-C_3N_4 (1.5 wt.%)/HAp for TC after three recycles was rather stable and remained about 100% (Fig. 7a), indicating that g-C_3N_4 (1.5 wt.%)/HAp photocatalyst possesses high stability and can be used for repeated treatment of TC. Moreover, the XRD diffraction patterns (Fig. 7b), FT-IR spectra (Fig. S6) and XPS spectra of (Fig. S7) g-C_3N_4 (1.5 wt.%)/HAp composite before and after TC degradation were further investigated. Note that the crystal structure and surface active groups of g-C_3N_4 (1.5 wt.%)/HAp composite have no obvious change even after the three successive photocatalytic reaction. Therefore, it can be concluded that the as-prepared g-C_3N_4 (1.5 wt.%)/HAp composite is reusable and stable in the photocatalytic process, and has a promising potential for practical application.

3.3. Photoelectrochemical properties of g-C_3N_4 (1.5 wt.%)/HAp photocatalyst

Transient photoelectrochemical response (PC) is an important technique to explore the photo-induced charge transfer and separation behaviors of g-C_3N_4 (1.5 wt.%)/HAp composite for the photodegradation of TC. In general, higher photocurrents reveal the effective separation of photo-generated charges, leading to higher photocatalytic activities. The photocurrent measurements of ultrathin g-C_3N_4, porous hollow HAp microspheres and g-C_3N_4 (1.5 wt.%)/HAp composite are shown in Fig. 8a. As expected, g-C_3N_4 (1.5 wt.%)/HAp shows a highest photocurrent intensity, much higher than ultrathin g-C_3N_4 and porous hollow HAp microspheres. The increasing photocurrent value of g-C_3N_4 (1.5 wt.%)/HAp demonstrates more photo-induced charge transfer efficiency and higher separation of the photo-generated electrons and holes, which is beneficial for the photocatalytic process.

Moreover, electrochemical impedance spectra (EIS) test is another effective way to analyze the transfer and separation of the photo-generated electrons and holes. Generally speaking, a smaller arc radius in EIS Nyquist plot indicates a higher efficiency of charge transfer and

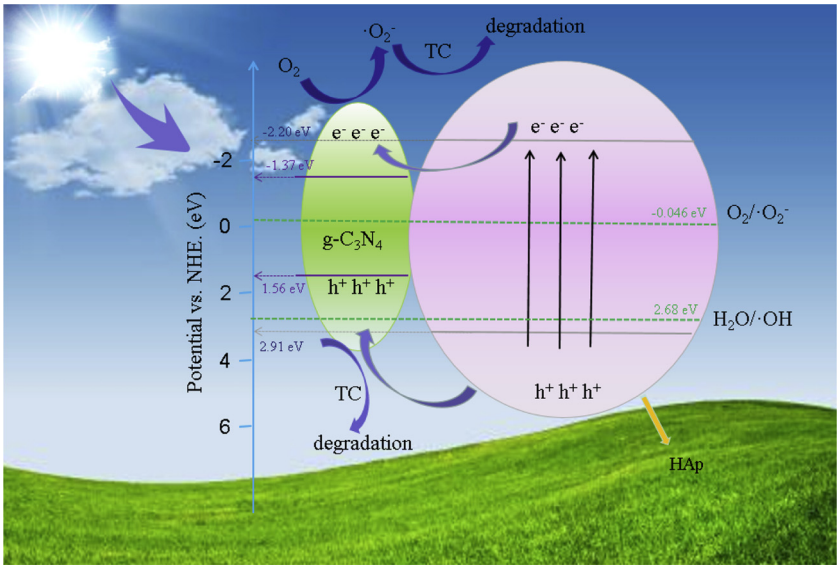

Fig. 10. Potential photocatalytic mechanism for the g-C_3N_4 (1.5 wt.%)/HAp composite under 300 W xenon lamp full spectrum irradiation.

lower recombination electron-hole pairs in a semiconductor. Fig. 8b displays the EIS Nyquist plots of the as-prepared ultrathin g-C_3N_4, porous hollow HAp microspheres, and g-C_3N_4 (1.5 wt.%)/HAp composite under the identical experimental conditions. Obviously, the arc radius of g-C_3N_4 (1.5 wt.%)/HAp composite in the EIS Nyquist plot was the smallest among these samples, indicating its highest charge transfer ability and separation efficiency of electron-hole pairs. The above point was well consistent with the result of photocurrent response.

3.4. Possible photocatalytic mechanism

As we know the superior photocatalytic performance of photocatalysts is attributed to the higher efficiency of charge separation and transfer of the photo-generated electron-hole pairs. In this research, UV–vis diffuse reflectance spectra (DRS) and Mott-Schottky (M-S) plots were carried out to determine the energy band structure and their electronic structures for porous hollow HAp microspheres and ultrathin g-C_3N_4 photocatalyst. The band gap energies (E_g) of indirect band-gap semiconductor can be calculated according to the plot of $(\alpha h\nu)^2$ versus photon energy (hv) [38]. As shown in Fig. S8, the E_g value of ultrathin g-C_3N_4 and porous hollow HAp microspheres was estimated to be 2.93 and 5.11 eV. The band-gap potentials for ultrathin g-C_3N_4 and porous hollow HAp microspheres were measured by Mott-Schottky (M-S) plots (Fig. S9) and then calculated as following:

$$EVB = ECB + Eg \quad (2)$$

In general, the conduction band (CB) potential of g-C_3N_4 semiconductors is higher than its flat band potential (ca. 0.20 V) [48].

To further investigate the mechanistic information, a series of tapping experiments (Fig. 9a) were carried out to detect the main active species during the photocatalytic process. Note that IPA, BQ, and EDTA were used as different scavenger for ·OH, $\cdot O_2^-$, and h^+ radical species, respectively. As can be seen from Fig. 9, with the addition of IPA into the reaction system, there was no decrease in the degradation efficiency, suggesting that ·OH is not a main active species in the present study. In contrast, the degradation efficiency was significantly reduced in the presence of BQ (from 100% to 21.3%), indicating that $\cdot O_2^-$ plays an important role in TC degradation process. Similarly, a significant loss could be observed (from 100% to 39.2%) when EDTA was employed for the scavenger in the reaction, verifying that h^+ is another crucial active species for TC removal. Thus, it can be inferred that both $\cdot O_2^-$ and h^+ are the main active species that responsible for the photocatalytic degradation of TC [49]. The above tapping experiments provide good proof for the photocatalytic mechanistic analysis.

In order to further confirm the above-obtained main active species during the photocatalytic process, the ESR analysis were performed and the corresponding results are shown in Fig. 9b–c. As expected, the obvious characteristic signals of the DMPO-$\cdot O_2^-$ (Fig. 9b) and TEMPO-h^+ (Fig. 9c) were detected for g-C_3N_4 (1.5 wt.%)/HAp under a 300 W xenon lamp full spectrum irradiation. Based on the analysis of tapping experiments and ESR characterization, it can be concluded that $\cdot O_2^-$ and h^+ active species play important roles in the photocatalytic process [50].

Based on the above experimental results, a possible photocatalytic mechanism of g-C_3N_4 (1.5 wt.%)/HAp composite photocatalyst is proposed, which can be explained in Fig. 10. As shown in Table S1, it should be noted that the CB potential of ultrathin g-C_3N_4 and porous hollow HAp microspheres are -1.37 V and -2.20 V. The CB potential of porous hollow HAp microspheres were more negative than the standard reduction potential of $O^2/\cdot O^{2-}$ (−0.046 V), the excited electrons in the CB could be easily trapped by molecular oxygen to form $\cdot O^{2-}$. And the VB potential (2.91 V) of porous hollow HAp microspheres were more positive than the standard reduction potential of $\cdot OH/H_2O$ (2.68 V) [51], the excited holes and electrons in the VB and CB move to g-C_3N_4 and effectively inhibit the photo-generated electron-hole pairs recombination [52,53]. Both $\cdot O_2$- and h^+ can directly degrade TC. As discussed, the presence of ultrathin g-C_3N_4 and porous hollow HAp microspheres in the g-C_3N_4/HAp composites promote the separation efficiency of the photogenerated electron-hole pairs, and thus resulting in high photocatalytic efficiency toward TC degradation.

4. Conclusion

In summary, a facile hydrothermal route was optimized for small amount of ultrathin g-C_3N_4 decorating on porous hollow HAp microspheres for the first time. The photocatalytic efficiencies of the as-prepared various g-C_3N_4/HAp composites were evaluated by degradation of TC under a 300 W xenon lamp full spectrum irradiation. The experimental results showed that porous hollow HAp microspheres decorated with small amount of ultrathin g-C_3N_4 can act as effective photocatalysts for TC degradation. Importantly, g-C_3N_4 (1.5 wt.%)/HAp composite displayed an excellent photocatalytic activity, which was faster than those over porous hollow HAp microspheres and ultrathin g-C_3N_4. In the meantime, g-C_3N_4 (1.5 wt.%)/HAp composite exhibited a good stability in the cyclic runs for TC degradation, confirming its promising potential as an efficient photocatalyst. The enhanced

photocatalytic ability could be ascribed to promotion the separation efficiency of the photogenerated electron-hole pairs. This research is expected to provide new insights to explore highly efficient and compatible photocatalyst that with potential application prospects.

Acknowledgements

This work was financially supported by the National Natural Science Foundation of China (21107069, 21103106), and the Science and Technology Commission of Shanghai Municipality (14DZ2261000).

Appendix A. Supplementary data

Supplementary material related to this article can be found, in the online version, at doi:https://doi.org/10.1016/j.apcatb.2019.01.020.

References

[1] H. Salle, D. De La, D. Hanau, A. Fricker, A. Urlacher, J. Kelly, S.H. Salamero, L. Powis, H. Donato, M. Bausinger, Laforet, Science 265 (1994) 237–241.
[2] B. Luo, D. Xu, D. Li, G. Wu, M. Wu, W. Shi, M. Chen, ACS Appl. Mater. Interfaces 7 (2015) 17061.
[3] C.I. Brinzila, N. Monteiro, M.J. Pacheco, L. Ciriaco, I. Siminiceanu, A. Lopes, Environ. Sci. Pollut. Res. Int. 21 (2014) 8457–8465.
[4] O. Hanay, B. Yildiz, S. Aslan, H. Hasar, Environ. Sci. Pollut. Res. Int. 21 (2014) 3774–3782.
[5] H. Shi, X. Xiao, L. Zeng, Q. Zhang, J. Nan, L. Wang, J. Nanosci. Nanotechnol. 14 (2014) 6934–6940.
[6] J. Liangliang, C. Wei, D. Lin, Z. Dongqiang, Environ. Sci. Technol. 43 (2009) 2322–2327.
[7] C.V. Gómez-Pacheco, M. Sánchez-Polo, J. Rivera-Utrilla, J. López-Peñalver, Chem. Eng. J. 178 (2011) 115–121.
[8] N. Oturan, J. Wu, H. Zhang, V.K. Sharma, M.A. Oturan, Appl. Catal. B Environ. 140-141 (2013) 92–97.
[9] Y. Liu, J. Kong, J. Yuan, W. Zhao, X. Zhu, C. Sun, J. Xie, Chem. Eng. J. 40 (2017) 10822.
[10] Q. Liu, J. Shen, X. Yang, T. Zhang, H. Tang, Appl. Catal. B Environ. 232 (2018) 562–573.
[11] I.D. Godos, R. Muñoz, B. Guieysse, J. Hazard. Mater. 229–230 (2012) 446–449.
[12] H. Kim, Y. Hong, J.E. Park, V.K. Sharma, S.I. Cho, Chemosphere 91 (2013) 888–894.
[13] M. Liu, Y. Zhang, M. Yang, Z. Tian, L. Ren, S. Zhang, Environ. Sci. Technol. 46 (2012) 7551.
[14] V.S. Bystrov, C. Piccirillo, D.M. Tobaldi, P.M.L. Castro, J. Coutinho, S. Kopyl, R.C. Pullar, Appl. Catal. B Environ. 196 (2016) 100–107.
[15] Masato Wakamura, A. Kazuhito Hashimoto, T. Watanabe, Langmuir 19 (2003) 3428–3431.
[16] T.S. Phan, A.R. Sane, B. Rêgo de Vasconcelos, A. Nzihou, P. Sharrock, D. Grouset, D. Pham Minh, Appl. Catal. B Environ. 224 (2018) 310–321.
[17] M. Reddy, A. Venugopal, M. Subrahmanyam, Appl. Catal. B: Environ. 69 (2007) 164–170.
[18] S. Kojima, F. Nagata, S. Kugimiya, K. Kato, Appl. Surf. Sci. 458 (2018) 438–445.
[19] X. Wang, L. Zhang, Q. Zeng, G. Jiang, M. Yang, Appl. Surf. Sci. 452 (2018) 381–388.
[20] R. Jiang, M. Liu, H. Huang, L. Huang, Q. Huang, Y. Wen, Q.-y. Cao, J. Tian, X. Zhang, Y. Wei, Appl. Surf. Sci. 434 (2018) 1129–1136.
[21] M. Prakash, T. Lemaire, D. Di Tommaso, N. de Leeuw, M. Lewerenz, M. Caruel, S. Naili, Appl. Surf. Sci. 418 (2017) 296–301.
[22] I. Papailias, N. Todorova, T. Giannakopoulou, N. Ioannidis, N. Boukos, C.P. Athanasekou, D. Dimotikali, C. Trapalis, Appl. Catal. B: Environ. 239 (2018) 16–26.
[23] Y. Liu, X. Xu, J. Zhang, H. Zhang, W. Tian, X. Li, M.O. Tade, H. Sun, S. Wang, Appl. Catal. B: Environ. 239 (2018) 334–344.
[24] J. Wang, J. Chen, P. Wang, J. Hou, C. Wang, Y. Ao, Appl. Catal. B: Environ. 239 (2018) 578–585.
[25] W. Zou, B. Deng, X. Hu, Y. Zhou, Y. Pu, S. Yu, K. Ma, J. Sun, H. Wan, L. Dong, Appl. Catal. B: Environ. 238 (2018) 111–118.
[26] L. Liang, Y. Cong, L. Yao, F. Wang, L. Shi, Mater. Res. Express 5 (2018) 115510.
[27] Y. Deng, L. Tang, C. Feng, G. Zeng, J. Wang, Y. Zhou, Y. Liu, B. Peng, H. Feng, J. Hazard. Mater. 344 (2018) 758–769.
[28] Y. Wang, M. Qiao, J. Lv, G. Xu, Z. Zheng, X. Zhang, Y. Wu, Fullerenes, Nanotubes and Carbon Nanostructures Vol. 26 (2018), pp. 210–217.
[29] M. Reddy, A. Venugopal, M. Subrahmanyam, Appl. Catal. B: Environ. 69 (2007) 164–170.
[30] X. Zhang, X. Zhang, J. Li, J. Sun, J. Bian, J. Wang, Y. Qu, R. Yan, C. Qin, L. Jing, Appl. Catal. B: Environ. 237 (2018) 50–58.
[31] W. Wang, G. Li, T. An, D.K.L. Chan, J.C. Yu, P.K. Wong, Appl. Catal. B: Environ. 238 (2018) 126–135.
[32] S. Gong, Z. Jiang, P. Shi, J. Fan, Q. Xu, Y. Min, Appl. Catal. B: Environ. 238 (2018) 318–327.
[33] W. Lai, C. Chen, X. Ren, I.-S. Lee, G. Jiang, X. Kong, Mater. Sci. Eng.: C 62 (2016) 166–172.
[34] X. Song, Y. Hu, M. Zheng, C. Wei, Appl. Catal. B: Environ. 182 (2016) 587–597.
[35] W. Wang, J. Fang, S. Shao, M. Lai, C. Lu, Appl. Catal. B: Environ. 217 (2017) 57–64.
[36] Y. Wang, F. Wang, Y. Feng, Z. Xie, Q. Zhang, X. Jin, H. Liu, Y. Liu, W. Lv, G. Liu, Dalton Trans. 47 (2017) 1284–1293.
[37] G. Xu, Y. Zhang, Y. Fu, Q. Guo, ACS Catal. 7 (2017) 1158–1169.
[38] Q. Liu, T. Chen, Y. Guo, Z. Zhang, X. Fang, Appl. Catal. B: Environ. 193 (2016) 248–258.
[39] T. Wang, C. Li, J. Ji, Y. Wei, P. Zhang, S. Wang, X. Fan, J. Gong, ACS Sustain. Chem. Eng. 2 (2014) 2253–2258.
[40] H. Zhang, L.H. Guo, D. Wang, L. Zhao, ACS Appl. Mater. Interfaces 7 (2015) 1816–1823.
[41] Z. Chen, F. Bing, Q. Liu, Z. Zhang, X. Fang, J. Mater. Chem. A 3 (2015) 4652–4658.
[42] Y. Zhang, Z.R. Tang, X. Fu, Y.J. Xu, ACS Nano 5 (2011) 7426–7435.
[43] F. Chen, Q. Yang, X. Li, G. Zeng, D. Wang, C. Niu, J. Zhao, H. An, T. Xie, Y. Deng, Appl. Catal. B: Environ. 200 (2017) 330–342.
[44] C. Cai, Z. Zhang, J. Liu, N. Shan, H. Zhang, D.D. Dionysiou, Appl. Catal. B: Environ. 182 (2016) 456–468.
[45] H. Wang, X. Yuan, Y. Wu, G. Zeng, X. Chen, L. Leng, H. Li, Appl. Catal. B: Environ. 174–175 (2015) 445–454.
[46] Y. Li, S. Wang, Y. Zhang, R. Han, W. Wei, J. Mol. Liq. 247 (2017) 171–181.
[47] W. Shi, F. Guo, S. Yuan, Appl. Catal. B: Environ. 209 (2017) 720–728.
[48] X. Li, J. Yu, J. Low, Y. Fang, J. Xiao, X. Chen, J. Mater. Chem. A 3 (2015) 2485–2534.
[49] T. Cai, Y. Liu, L. Wang, S. Zhang, Y. Zeng, J. Yuan, J. Ma, W. Dong, C. Liu, S. Luo, Appl. Catal. B 208 (2017) 1–13.
[50] Y. Bao, K. Chen, Appl. Surf. Sci. 437 (2018) 51–61.
[51] T. Na, H.W. Huang, H. Ying, Y. Guo, T. Zhang, Dalton Trans. 44 (2015) 4297–4307.
[52] J. Lyu, J. Shao, Y. Wang, Y. Qiu, J. Li, T. Li, Y. Peng, F. Liu, Chem. Eng. J. 358 (2019) 614–620.
[53] C. Lai, M. Zhang, B. Li, D. Huang, G. Zeng, L. Qin, X. Liu, H. Yi, M. Cheng, L. Li, Z. Chen, L. Chen, Chem. Eng. J. 358 (2019) 891–902.